Available online at www.sciencedirect.com
ScienceDirect
Geochimica et Cosmochimica Acta 71 (2007) 531–542
Geochimica
www.elsevier.com/locate/gca

Modeling the kinetics of silica nanocolloid formation and precipitation in geologically relevant aqueous solutions

Christine F. Conrad [a,*], Gary A. Icopini [b,1], Hideaki Yasuhara [c,2], Joel Z. Bandstra [a], Susan L. Brantley [a,b], Peter J. Heaney [a,b]

[a] *Center for Environmental Kinetics Analysis, The Pennsylvania State University, University Park, PA 16802, USA*
[b] *Department of Geosciences, The Pennsylvania State University, University Park, PA 16802, USA*
[c] *The Energy Institute, The Pennsylvania State University, University Park, PA 16802, USA*

Received 11 May 2006; accepted in revised form 2 October 2006

Abstract

The kinetics of the formation and precipitation of nanocolloidal silica from geologically relevant aqueous solutions is investigated. Changes in monomeric ($SiO_{2(mono)}$), nanocolloidal ($SiO_{2(nano)}$) and precipitated silica ($SiO_{2(ppt)}$) concentrations in aqueous solutions from pH 3 to 7, ionic strengths (IS) of 0.01 and 0.24 molal, and initial SiO_2 concentrations of 20.8, 12.5 and 4.2 mmolal (reported in [Icopini, G.A., Brantley, S.L., Heaney, P.J., 2005. Kinetics of silica oligomerization and nanocolloid formation as a function of pH and ionic strength at 25 °C. *Geochim. Cosmochim. Acta* **69**(2), 293–303.]) were fit using two kinetic models. The first model, termed the concentration model, is taken from Icopini et al. (2005) and assumes that the rate of change of $SiO_{2(mono)}$ as a function of time has a fourth-order dependence on the concentration of $SiO_{2(mono)}$ in solution. The second model, termed the supersaturation model, incorporates the equilibrium concentration of amorphous silica and predicts that polymerization will be a function of the degree of silica supersaturation in solution with respect to amorphous silica. While both models generally predicted similar rate constants for a given set of experimental conditions, the supersaturation model described the long-term equilibrium behavior of the $SiO_{2(mono)}$ fraction more accurately, resulting in significantly better fits of the monomeric data. No difference was seen between the model fits of the nanocolloidal silica fraction. At lower pH values (3–4), a metastable equilibrium was observed between $SiO_{2(mono)}$ and $SiO_{2(nano)}$. This equilibrium $SiO_{2(mono)}$ concentration was found to be 6 mmolal, or three times the reported solubility of bulk amorphous silica under the experimental conditions studied and corresponds to the predicted solubility of amorphous silica colloids approximately 3 nm in diameter. Atomic force microscopy was used to determine the average size of the primary nanocolloidal particles to be ~3 nm, which is in direct agreement with the solubility calculations. Larger aggregates of the primary nanocolloids were also observed to range in size from 30 to 40 nm. This work provides the first kinetic models describing the formation and evolution of nanocolloidal silica in environmentally relevant aqueous solutions. Results indicate that nanocolloidal silica is an important species at low pH and neutral pH at low ionic strengths and may play a more important role in geochemical cycles in natural aqueous systems than previously considered.

1. Introduction

In soils and natural waters, the solid–water interfaces of colloids can regulate the concentrations of most reactive elements and of many pollutants. Colloid surfaces control aggregation reactions, act as redox catalysts and play an important role in the uptake and transport of nutrients and contaminant materials (Brown et al., 1999). The size,

* Corresponding author.
E-mail addresses: cfc11@psu.edu (C.F. Conrad), gicopini@mtech.edu (G.A. Icopini), hide@dpc.ehime-u.ac.jp (H. Yasuhara), jxb88@psu.edu (J.Z. Bandstra), brantley@geosc.psu.edu (S.L. Brantley), pjh14@psu.edu (P.J. Heaney).
[1] Present address: Montana Bureau of Mines and Geology, Montana Tech of the University of Montana, Butte, Montana, 59701-8997, USA.
[2] Present address: Ehime University, Department of Civil and Environmental Engineering, Matsuyama 790-8577, Japan.

0016-7037/$ - see front matter © 2006 Elsevier Inc. All rights reserved.
doi:10.1016/j.gca.2006.10.001

shape and composition of colloids can also have a profound effect on their function as a catalyst or sol–gel in industrial applications. The growth and nucleation of silica nanocolloids is especially interesting as they are ubiquitous in nature and the mechanism by which they grow and precipitate is essential to understanding a variety of geologic processes. Silica reaction kinetics play a critical role in thermally enhanced oil recovery and subsurface contamination remediation, disposal of reactive waste by burial and geothermal waste-waters by injection into the subsurface (Carroll et al., 1998).

Despite the extensive characterization of the silica system, few studies have examined the formation of silica in fluids of geologic significance with relatively low silica concentrations, varying ionic strengths and the full natural pH range. Even fewer studies have characterized the kinetics of the formation and growth of the nanocolloidal phase. Most research investigating the formation of silica nanocolloids has been directed at the production of materials for industrial applications. Methods for synthesizing monodisperse colloidal silica through techniques such as the Stöber method are well established (Bogush and Zukoski, 1991; Van Blaaderen et al., 1992; Arriagada and Osseo-Asare, 1999; Pontoni et al., 2002) and sophisticated models have been derived to describe the growth of these particles over time (for example, Lee et al., 1998). Additionally, characterization techniques such as small angle X-ray scattering (SAXS) have provided detailed information as to the growth mechanism and changes in the physical and chemical properties of these Stöber particles over time (Boukari et al., 1997; Pontoni et al., 2002). Conversely, silica colloids formed at low degrees of supersaturation from aqueous solutions are often amorphous particles of such low density that traditional characterization techniques are unable to provide reliable information as to changes in particle size, shape and porosity. Therefore, the application of more sophisticated aggregation models is hindered in these systems.

In this study, we extend our previous work (Icopini et al., 2005) by applying kinetic models to determine both rate constants for the conversion of monomeric to nanocolloidal silica (k_1) and the subsequent conversion of nanocolloidal silica to the precipitated form (k_2). The overall reaction of the silica precipitation process can be defined as:

$$SiO_{2(mono)} \xrightarrow{k_1} SiO_{2(cn)} \xrightarrow{k_{fast}} SiO_{2(nano)} \xrightarrow{k_2} SiO_{2(ppt)} \quad (1)$$

where silica follows the general behavior observed for precipitation in closed systems; the supersaturation in solution declines as monomeric silica ($SiO_{2(mono)}$) nucleates and grows to a critical nucleus ($SiO_{2(cn)}$) whose size may vary depending on the experimental conditions (Rajasekaran et al., 2003; Izumi et al., 2005; Madras and McCoy, 2005). The critical nucleus is defined as the smallest cluster of molecules or atoms needed for growth to continue spontaneously. Once the critical nucleus is formed, oligomerization rapidly continues to form a nanocolloidal phase ($SiO_{2(nano)}$). Primary nanocolloidal silica particles have been shown to be 3 nm in diameter and consist of approximately 300 silica monomer units under the conditions of our experiments (Icopini et al., 2005). Continued growth of the nanocolloidal phase through some mechanism such as coalescence or aggregation results in precipitation ($SiO_{2(ppt)}$). In this study, precipitated silica is defined as particles that do not pass through a 0.1 μm filter. The rates of these processes can be described by the rate constants k_1 (oligomerization) and k_2 (precipitation) as shown in Eq. (1).

Icopini et al. (2005) investigated the initial stages of silica oligomerization and nanocolloid formation (i.e., k_1) in solutions from pH 3 to 11 in a low ionic strength solution (0.01 molal) and a geothermal brine (0.24 molal). The work presented in this paper builds upon the previous results by (1) extending the model employed by Icopini et al. (2005) to fit silica precipitation (i.e., k_2), and (2) to fit silica oligomerization and precipitation using a modified kinetic model based on Goto (1956). Whereas the focus of Icopini et al. (2005) was to characterize the formation of the nanocolloidal silica fraction by investigating the disappearance of monomeric silica, the primary focus of this work is to determine not only what factors affect the rate of nanocolloidal silica formation, but also to examine nanocolloid conversion to precipitated silica. Understanding the conditions under which nanocolloidal silica forms and persists will allow for a more complete understanding of the environments in which these particles should be considered important in geochemical studies.

1.1. Concentration model

The first model we tested is taken directly from Icopini et al. (2005) and assumes that the rate of polymerization of silica is directly proportional to the concentration of monomeric SiO_2 in solution. This model will be termed the "concentration model" for the purpose of this study. The rate of decrease in molybdate-reactive (or "monomeric") silica with time was observed to be fourth-order leading to the following rate equation

$$\frac{d[SiO_{2(mono)}]}{dt} = -k_1[SiO_{2(mono)}]^4 \quad (2)$$

where k_1 is the reaction rate constant for the formation of the critical nucleus. Details of the derivation of this model and its fourth-order dependence can be found in Icopini et al. (2005). Note that Icopini et al. (2005) used the initial rate method to determine rate constants for the conversion of $SiO_{2(mono)}$ to $SiO_{2(nano)}$ and only utilized a subset of the entire dataset. Because we are interested in the long term behavior of the nanocolloidal fraction, we have utilized the entire data set for fitting resulting in slightly different rate constants reported here.

To develop this model so as to incorporate precipitation, we assume that the growth of the critical nucleus to the nanocolloid phase is fast, but that the reaction from the

nanocolloid to the precipitate (rate constant k_2) is slow. Thus, the change in nanocolloidal silica concentrations with time may be described as in Eq. (3) as the difference between the growth of $SiO_{2(nano)}$ from critical nuclei formed by $SiO_{2(mono)}$ (assumed to be fourth-order as shown by Icopini et al., 2005) and the loss of $SiO_{2(nano)}$ through the formation of $SiO_{2(ppt)}$:

$$\frac{d[SiO_{2(nano)}]}{dt} = \frac{1}{4}k_1[SiO_{2(mono)}]^4 - k_2[SiO_{2(nano)}]^m \quad (3)$$

where k_1 is the reaction rate constant for the formation of critical nuclei, k_2 is the reaction rate constant for the conversion of $SiO_{2(nano)}$ to $SiO_{2(ppt)}$, and m is the reaction order with respect to $SiO_{2(nano)}$.

1.2. Supersaturation model

The second model we tested was originally formulated by Goto (1956) to describe the loss of monomeric silica from aqueous solution by incorporating a term for the solubility of amorphous silica at a given temperature. For the fourth-order reaction observed by Icopini et al. (2005), the rate equation for the change in $SiO_{2(mono)}$ over time using the supersaturation model is expressed in Eq. (4). Substituting this expression into Eq. (3) gives the rate equation for $SiO_{2(nano)}$ Eq. (5).

$$\frac{d[SiO_{2(mono)}]}{dt} = -k_1[SiO_{2(mono)} - SiO_{2(eq)}]^4 \quad (4)$$

$$\frac{d[SiO_{2(nano)}]}{dt} = \frac{1}{4}k_1[SiO_{2(mono)} - SiO_{2(eq)}]^4 - k_2[SiO_{2(nano)}]^m \quad (5)$$

The reaction rate constants k_1 and k_2 describe the formation of the critical nucleus and the rate of precipitation, respectively, and m is the reaction order with respect to $SiO_{2(nano)}$. $SiO_{2(eq)}$ is the equilibrium solution concentration of amorphous silica at a given temperature and is generally reported to be approximately 2.0 mmolal at 25 °C (Weres et al., 1981; Icenhower and Dove, 2000). However, the solubility of amorphous silica can vary as a function of pH with a higher solubility at acidic pHs (~2.5 mmolal at pH 3) and lower solubility at neutral pH (~1.7 mmolal at pH 7) (Alexander, 1954; Iler, 1979). In this model, the rate of reaction is dependent not only on the initial concentration of $SiO_{2(mono)}$, but also on the degree of supersaturation with respect to amorphous SiO_2. It is assumed that conversion to critical nuclei will occur as long as the concentration of monomeric SiO_2 is greater than the equilibrium concentration of amorphous SiO_2.

2. Experimental

2.1. Batch experiments

The silica oligomerization and precipitation data fit in this work are the result of experiments reported in Icopini et al. (2005). Briefly, stock solutions of aqueous SiO_2 were prepared by dissolving 10.593 g $Na_2SiO_2{\cdot}5H_2O$ in 500 mL distilled, deionized water. Sodium was removed with a cation exchange resin (Dowex 50W-X8, 20–50 mesh, H-form) reducing the pH to <3. The solution was then filtered and the pH raised to >10.85 with 1 M NaOH. Oligomerization of silica was studied at a low ionic strength (0.01 molal) and in a high ionic strength (0.24 molal) brine solution (200 millimolal Na^+, 25.1 millimolal K^+, 5.00 millimolal Ca^{2+}, 236 millimolal Cl^-, 0.739 millimolal HCO_3^-; geothermal and power operations, Unocal Corporation; Gallup, 1997). Initial $SiO_{2(TD)}$ values of 4.2, 12.5 and 20.8 millimolal were chosen to encompass the range of concentrations most often observed in geothermal fluids and natural aqueous systems (Rothbaum and Anderton, 1975; Gudmundson and Einarsson, 1989; Vitolo and Cialdella, 1994; Gallup, 1997; Willey and Spivak, 1997; Miretzky et al., 2001; Ding et al., 2004). The concentrations of $SiO_{2(mono)}$, $SiO_{2(nano)}$, and $SiO_{2(ppt)}$ were monitored over a period of 96 h (high IS) and 2808 h (low IS). The concentration of $SiO_{2(nano)}$ was calculated as the difference between $SiO_{2(TD)}$ measured using ICP-AES in solutions filtered through a 0.1 μm filter (TF Puradisc, Whatman) and $SiO_{2(mono)}$ measured using the colorimetric molybdate-blue method (U.S.G.S., 1989). $SiO_{2(ppt)}$ was quantified as the difference between the initial silica concentration and $SiO_{2(TD)}$ of the filtered solutions.

A new, separate experiment was conducted using the methods described above to image the silica nanocolloids formed in solutions with 20.8 mmolal SiO_2 at low IS. The solution was reacted at pH 7 for 12 h to produce a sufficient concentration of nanocolloidal silica in suspension. After 12 h, the pH of the experimental solution was adjusted to pH 3 to freeze the reaction. Precipitated silica was removed by filtering through a 0.1 μm filter and the remaining solution was dropped on an atomically smooth silicon wafer. After a 20-min deposition, excess solution was wicked away by gently touching a tissue to the corner of the wafer. Images were obtained in air using a Digital Instruments Dimension 3000 AFM in tapping mode with a scan speed of 1 Hz, 512 samples/line and a Si-sharpened tip with a tip radius ⩽10 nm.

2.2. Numerical methods

Reaction rate constants were obtained by fitting the integrated forms of Eq. (2) through (5) to the silica species concentration vs. time data using Levenberg–Marquardt square error minimization (Press et al., 1992). In the present study, the data were refit to the same model used in Icopini et al. (2005) (i.e., the concentration model) and to the new (supersaturation) model. Note that Icopini et al. (2005) employed the initial rate method to determine the rate of oligomerization and therefore used only a subset of the data. The objective of this study is to predict long-term behavior including the formation and growth of the nanocolloidal phase requiring use of the

entire data set. This results in slightly different values for k_1 presented here for the concentration model from those reported in Icopini et al. (2005). Closed-form fitting equations for $SiO_{2(mono)}$ were obtained by direct integration of Eqs. (2) and (4) yielding the following for the concentration model Eq. (6) and supersaturation model Eq. (7).

$$[SiO_{2(mono)}] = \left(\frac{1}{3k_1t + (1/[SiO_{2(mono)}]_{t=0}^3)}\right)^{1/3} \quad (6)$$

$$[SiO_{2(mono)}] = \left(3k_1t + \frac{1}{([SiO_{2(mono)}]_{t=0} - [SiO_{2(eq)}])^3}\right)^{-1/3} + [SiO_{2(eq)}] \quad (7)$$

where $[SiO_{2(mono)}]_{t=0}$ is the initial concentration of monomeric SiO_2 and $SiO_{2(eq)}$ is the equilibrium concentration of amorphous SiO_2 at a given temperature. These equations were then substituted into Eqs. (3) and (5) to obtain the following for the concentration model Eq. (8) and the supersaturation model Eq. (9), respectively.

$$\frac{d[SiO_{2(nano)}]}{dt} = \frac{1}{4}k_1\left(\frac{1}{3k_1t + (1/[SiO_{2(mono)}]_{t=0}^3)}\right)^{4/3} - k_2[SiO_{2(nano)}]^m \quad (8)$$

$$\frac{d[SiO_{2(nano)}]}{dt} = \frac{1}{4}k_1\left[\left(3k_1t + \frac{1}{([SiO_{2(mono)}]_{t=0} - [SiO_{2(eq)}])^3}\right)^{-1/3} + [SiO_{2(eq)}]\right]^4 - k_2[SiO_{2(nano)}]^m \quad (9)$$

Closed-form solutions for $SiO_{2(nano)}$ are not available. Therefore, Eqs. (8) and (9) were integrated numerically using the fourth-order Runge–Kutta–Fehlberg method.

The rate constant k_1 was fit by guessing values for $[SiO_{2(mono)}]_{t=0}$, $[SiO_{2(eq)}]$ and k_1 and optimizing the fitting function. For a given experimental condition (e.g., pH, ionic strength, $SiO_{2(TD)}$), $[SiO_{2(mono)}]_{t=0}$, the fitted k_1 is then substituted into the corresponding equations and held constant to determine the best fit of k_2. Parameters $[SiO_{2(mono)}]_{t=0}$ and $[SiO_{2(eq)}]$ were also allowed to float in fitting k_2. The numerical fits are compared with the experimental $SiO_{2(nano)}$, and the sum of squares is minimized. Fits of $SiO_{2(nano)}$ were carried out with reaction orders $m = 1$, 2, 3 and 4 to determine the most probable reaction order for the process of condensation of nanocolloidal to precipitated silica. Results from both the concentration and steady state models indicate that increasing m above 1 does not consistently enhance the fits (not shown). Therefore, for all fitting routines of $d[SiO_{2(nano)}]/dt$, $m = 1$ Eqs. (8) and (9). Model output concentrations of $SiO_{2(ppt)}$ were calculated by mass balance between the measured total dissolved silica ($[SiO_{2(TD)}]_{meas}$) and the fitted concentrations of $SiO_{2(mono)}$ and $SiO_{2(nano)}$ from the corresponding model:

$$[SiO_{2(ppt)}]_{Conc,SS} = [SiO_{2(TD)}]_{meas} - [SiO_{2(mono)}]_{Conc,SS} - [SiO_{2(nano)}]_{Conc,SS} \quad (10)$$

where the subscripts *Conc* and *SS* indicate which model was used to predict the given values.

3. Results

3.1. Silica concentrations

Two distinct trends were observed in the concentrations of the individual silica fractions in these experiments. At low pH (3–4) at both high and low ionic strengths for initial SiO_2 concentrations of 20.8 and 12.5 mmolal, a fast initial decrease in $SiO_{2(mono)}$ was followed by the establishment of an apparent steady state between $SiO_{2(mono)}$ and $SiO_{2(nano)}$ with little $SiO_{2(ppt)}$ forming (representative data shown in Fig. 1). Under these conditions, the concentration of the $SiO_{2(mono)}$ fraction approached 6 mmolal SiO_2. The stability of $SiO_{2(nano)}$, or the length of time nanocolloids are present before they react to form $SiO_{2(ppt)}$, was greatest at these conditions with nanocolloid lifetimes observed to be >2800 h (Fig. 1b and e). In contrast, at pH 5 and 6 for both low and high IS solutions and initial SiO_2 concentrations of 20.8 and 12.5 mmolal, the $SiO_{2(nano)}$ fraction was rapidly converted to $SiO_{2(ppt)}$ and the concentration of the $SiO_{2(mono)}$ fraction approached 2 mmolal SiO_2. This concentration is consistent with the reported amorphous silica solubility concentration at 25°C for solutions of the compositions studied here (Weres et al., 1981; Icenhower and Dove, 2000) (Fig. 2). Observed lifetimes for nanocolloidal silica at these latter conditions were typically ~1 to 12 h (Fig. 2b and e). Complete experimental data for the concentrations of monomeric, nanocolloidal and precipitated SiO_2 over time can be found in electronic annex EA-1.

3.2. Nanocolloidal silica

AFM images of the silica nanocolloids prepared at pH 7, an initial SiO_2 concentration of 20.8 mmolal and low IS show two distinct particle sizes (Fig. 3). These conditions were chosen to maximize the presence and concentration of the nanocolloid fraction in solution. The particles were imaged after a 12-h reaction period, but images of particles formed under the same experimental conditions for 1, 4 and 24 h reaction times showed a similar size distribution. The smallest individual particles in the image have a vertical dimension of ~3 nm. Because the AFM tip used to image these particles has a radius of 10 nm, particles smaller than

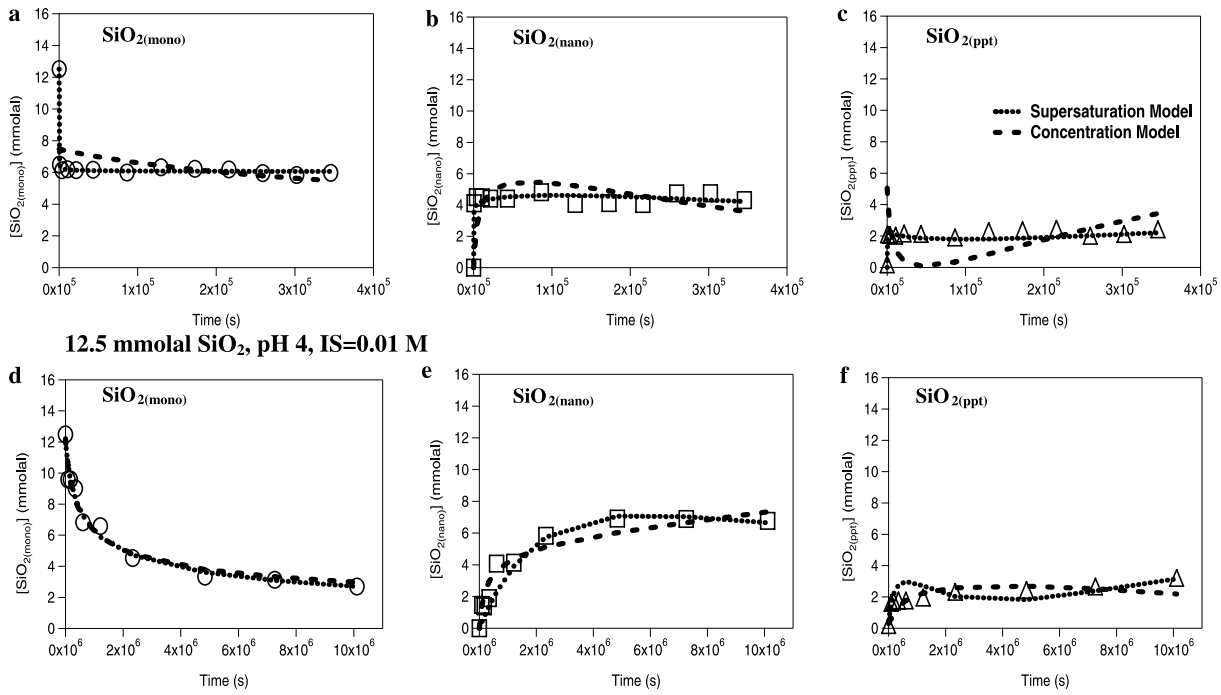

Fig. 1. Representative fits of the supersaturation and concentration models for 12.5 mmolal SiO_2 solutions at pH 4 for high (top) and low ionic strengths (bottom). Experimental data (open symbols) and fits (lines) are shown for (a and c) monomeric, (b and d) nanocolloidal, and (c and f) precipitated silica.

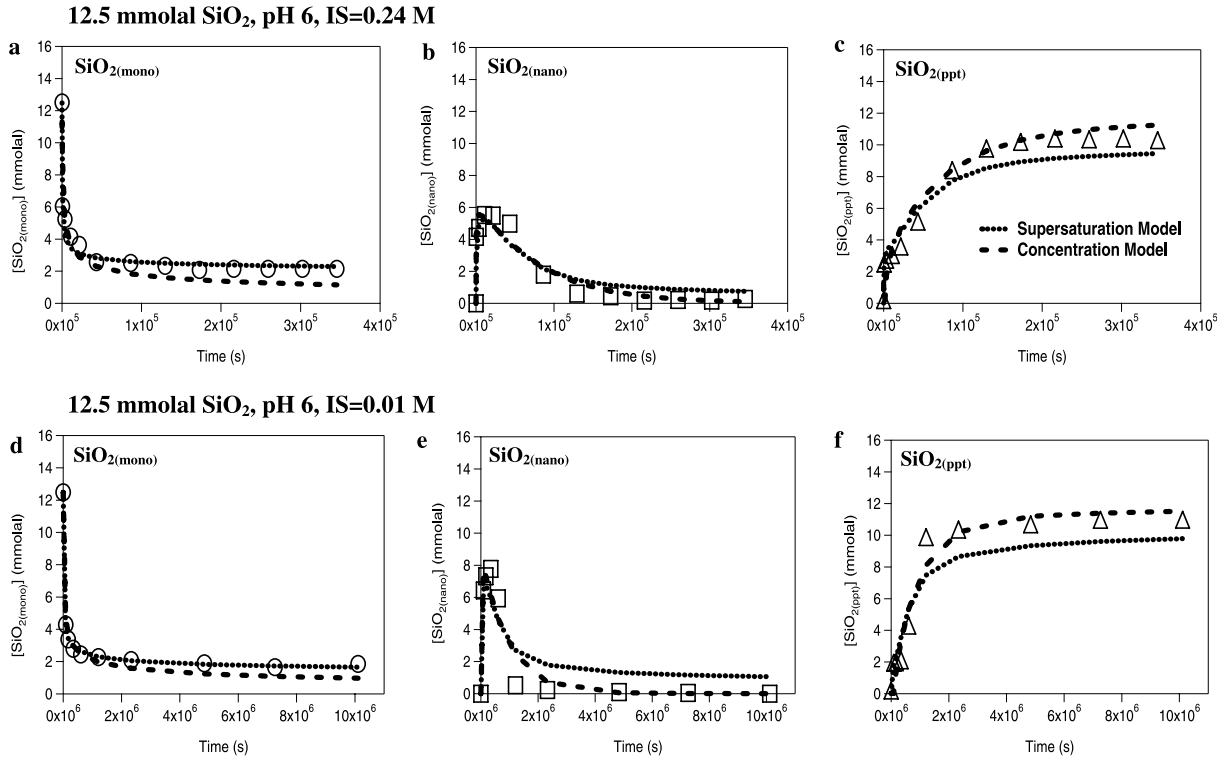

Fig. 2. Representative fits of the supersaturation and concentration models for 12.5 mmolal SiO_2 solutions at pH 6 for high (top) and low ionic strengths (bottom). Experimental data (open symbols) and fits (lines) are shown for (a and c) monomeric, (b and d) nanocolloidal, and (c and f) precipitated silica.

10 nm will have exaggerated dimensions in the x–y plane. However, the z-dimension can be measured very precisely, and assuming that the particles are spherical, the 3 nm height is a reliable measure of the nanocolloid diameter. The larger particles in the image are 30–40 nm in height and appear to consist of aggregates of the smaller primary particles.

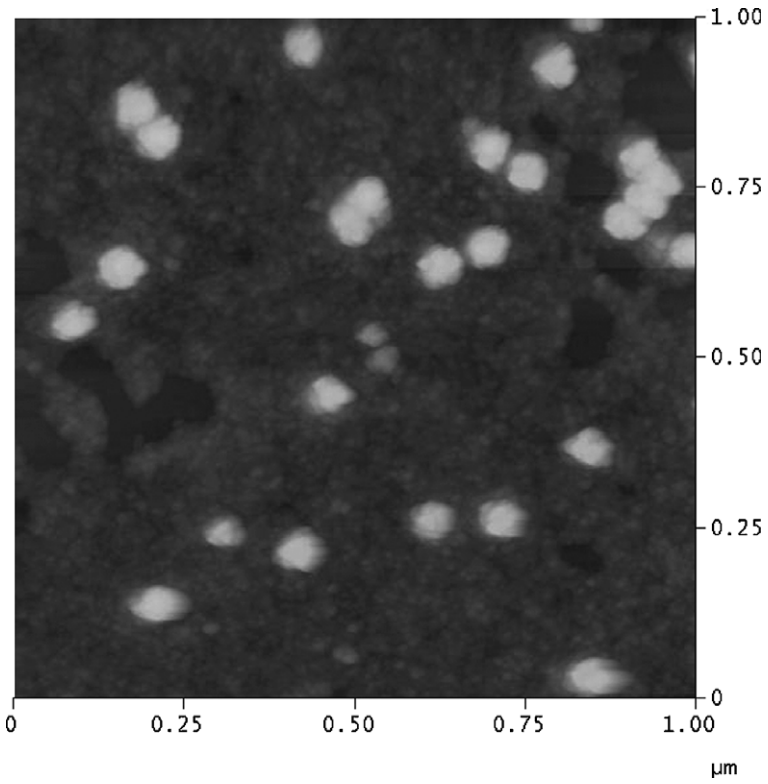

Fig. 3. AFM image (1 × 1 μm) of nanocolloidal silica fraction deposited on a silicon wafer from an experimental solution prepared at pH 7, an initial [SiO_2] of 20.8 mmolal and low IS. Particles are assumed to be spherical with the diameter measured in the *z*-direction. The smallest particles in the image are ~3 nm. The larger particles are 30–40 nm and are aggregates comprised of the 3 nm primary nanocolloids.

3.3. Reaction rate constants

3.3.1. Concentration model

The k_1 values determined using the entire data set followed the same general trends as those reported by Icopini et al. (2005). The largest values of k_1 were seen at initial SiO_2 concentrations of 20.8 mmolal and at near-neutral pH (Table 1). The same trend was seen in the high IS solutions. Note that the actual values of the rate constants reported here differ slightly from those reported by Icopini et al. (2005) as the entire data set was used in this work. As was seen in the previous work, values of the predicted log k_1 varied linearly with pH (Fig. 4a–c). In the 20.8 mmolal solutions, the degree of supersaturation outweighed the ionic strength effects as the reaction rate constants were similar for both high and low IS solutions over the pH range studied (Fig. 4a). The effect of ionic strength became more apparent at an initial silica concentration of 12.5 mmolal. Here, the log k_1 values for the high IS solutions were always higher than the log k_1 values for the low IS solutions (Fig. 4b). No ionic strength effects were seen at the lowest initial silica concentration due to the extremely slow rates of polymerization regardless of pH or IS (Fig. 4c).

The largest rate constants for the precipitation of nanocolloidal SiO_2 were also seen at initial SiO_2 concentrations of 20.8 mmolal and at near-neutral pH (Table 2). While the values of log k_1 varied linearly with pH, a similar trend was not generally seen in the log k_2 values (Fig. 4d–f). Only solutions with an initial SiO_2 concentration of 20.8 mmolal showed a linear correlation between pH and log k_2 values (Fig. 4d). Rate constants were similar for both the low and high IS solutions with initial SiO_2 concentrations of 20.8 mmolal indicating that the overall behavior was driven by the degree of supersaturation (Fig. 4d). Values determined for k_2 were generally 2–3 orders of magnitude higher than values of k_1 for comparable experimental conditions.

3.3.2. Supersaturation model

Rate constants predicted using the supersaturation model were generally in good agreement but were slightly faster than those predicted from the concentration model (Tables 1 and 2). The main exceptions to this occurred at low pH (3–4) and at high IS. Under these conditions, the difference in the predicted rate constants between the two models was up to 7 orders of magnitude (Table 1). Overall, values of k_1 ranged from 2.88×10^{-10} to 6.96×10^{-5} $mmol^{-3}\,s^{-1}$ and from 2.57×10^{-8} to 6.28×10^{-2} $mmol^{-3}\,s^{-1}$ for the 0.01 and 0.24 molal samples, respectively (Table 1). However, significant error in the fits of the experimental data at pH 3 and 4 in the high ionic strength solutions may have resulted in artificially high rate constants for this model. Under these conditions, an initial, instantaneous decrease in $SiO_{2(mono)}$ was followed by no significant change in $SiO_{2(mono)}$ concentration (Fig. 1a). Thus, the kinetics are

Table 1
Rate constants for the formation of nanocolloidal silica (k_1) as predicted by the concentration and supersaturation models

Initial [$SiO_{2(TD)}$] (mmolal)	IS (molal) (±10%)	pH (±0.2)	Concentration model k_1 ($\times 10^{-8}$) ($mmolal^{-3}\ s^{-1}$) (±standard error of fit)	Supersaturation model k_1 ($\times 10^{-7}$) ($mmolal^{-3}\ s^{-1}$) ±standard error of fit)
20.8	0.01	3	6.38 (2.17)	4.96 (4.38)
		4	10.6 (13.3)	1.84 (0.449)
		5	82.8 (19.6)	40.7 (4.62)
		6	186 (74.8)	696 (227)
		7	192 (72.3)	655 (197)
12.5	0.01	3	0.0195 (0.00346)	0.00288 (.00339)
		4	0.123 (0.0166)	0.00845 (0.00372)
		5	0.627 (0.0846)	0.522 (0.170)
		6	3.58 (0.741)	1.35 (0.267)
		7	7.10 (2.69)	19.3 (5.98)
4.2	0.01	3	0.135 (0.125)	.0601 (9.84)
		4	0.115 (0.156)	0.108 (26.8)
		5	0.354 (0.154)	0.0520 (2.24)
		6	0.382 (0.172)	0.0501 (2.15)
		7	1.55 (0.585)	0.0101 (0.297)
20.8	0.24	3	0.497 (0.437)	628,000 (230,000)[a]
		4	2.47 (1.82)	1,330 (1,860)[a]
		5	67.3 (32.7)	65.8 (42.5)
		6	143 (46.0)	56.9 (12.3)
		7	575 (342)	1,400 (295)
12.5	0.24	3	0.220 (0.248)	336,000 (268,000)[a]
		4	0.353 (0.279)	109,000 (70,500)[a]
		5	7.64 (3.54)	153 (131)
		6	62.7 (25.6)	65.8 (27.3)
		7	328 (166)	498 (93.7)
4.2	0.24	3	0.422 (0.208)	0.750 (22.5)
		4	0.363 (0.349)	3.22 (143)
		5	1.28 (0.374)	47.6 (204)
		6	0.450 (0.378)	1.95 (79.6)
		7	2.57 (0.418)	0.257 (0.140)

[a] The kinetics of these data were not well-defined resulting in poor fits. Consequently, these data were not included in the linear regression analyses of the log rate constant vs. pH.

not sufficiently resolved to predict the rate constants accurately for these samples and they are not included in the following discussion or data analysis.

The highest rates of reaction for both the low and high IS solutions were seen at an initial SiO_2 concentration of 20.8 mmolal and pH 6–7. The $\log k_1$ values varied linearly with pH for solutions with initial silica concentration of 12.5 and 20.8 mmolal (Fig. 5). As was seen in the concentration model results, the $\log k_1$ values for both the low and high IS solutions are similar and the degree of supersaturation drives the growth of the nanocolloids in the 20.8 mmolal solutions (Fig. 5a). Ionic strength effects become more apparent in the 12.5 mmolal solutions (Fig. 5b). No linear trend with pH was seen for the 4.2 mmolal silica solution (Fig. 5c).

Predicted k_2 values were also in good agreement with those determined using the concentration model. Rate constants ranged from 5.09×10^{-8} to 5.48×10^{-4} for the low IS solutions and from 1.37×10^{-6} to 7.12×10^{-4} for the high IS solutions (Table 2). At low IS, rates of precipitation were generally fastest at pH 5–6 and 20.8 mmolal SiO_2. At the higher ionic strength, the fastest rates of precipitation were seen at pH 7 and 20.8 mmolal SiO_2. As with the concentration model, the relationship between $\log k_2$ and pH was only observed for solutions with initial silica concentrations of 20.8 mmolal (Fig. 5d).

4. Discussion

In supersaturated solutions, oligomerization of monomeric silica to form stable nuclei of a critical size is the first step in the precipitation process. Once critical nuclei form they spontaneously grow to form spherical particles (Iler, 1979; Perry and Keeling-Tucker, 2000). The focus of this work was to predict the evolution of the concentrations of monomeric and, for the first time, nanocolloidal and precipitated silica over time as a function of pH, ionic strength, and initial SiO_2 concentration.

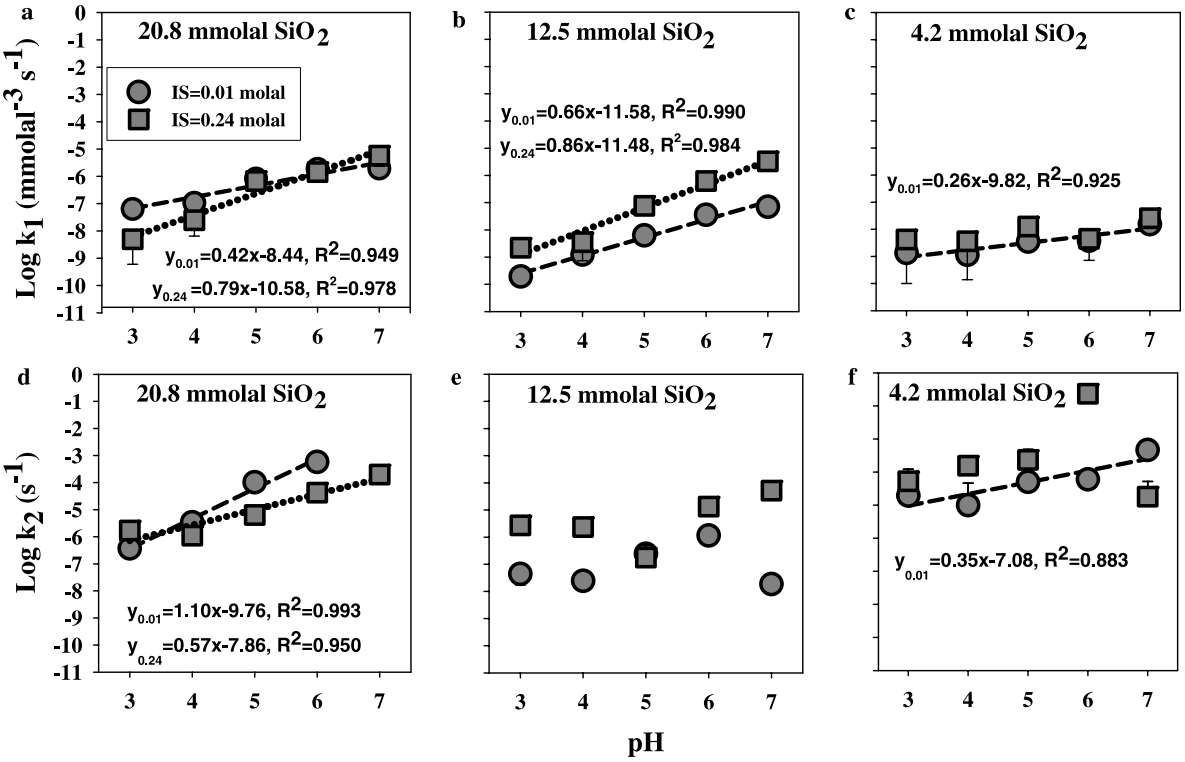

Fig. 4. Logk_1 (top panels) and log k_2 (bottom panels) values determined from the concentration model vs. pH for low ionic strength (circles) and high ionic strength (squares) experiments with initial SiO_2 concentrations of (a) 20.8, (b) 12.5 and (c) 4.2 mmolal. Error bars are one standard deviation of the predicted rate constant (when not shown, error bars are on the same scale as the data symbol). Open data symbols represent systems where the kinetics are not sufficiently resolved to predict the reaction rate constants accurately and were not included in the linear fits. Where linear regressions were found to be significant ($p < 0.05$), the equation and correlation coefficient are shown.

4.1. Model comparison

While both the concentration and supersaturation models produced similar results for the rates of polymerization of $SiO_{2(mono)}$ (k_1), significant differences in the ability of each model to fit the experimental data were seen. Fitting the disappearance of monomeric SiO_2 with the supersaturation model always resulted in smaller reduced χ^2 values that were often up to 10 times lower than those for fits from the concentration model. A complete comparison of reduced χ^2 parameters for the two models can be found in electronic annex EA-2. The concentration model often over-estimated the extent of polymerization of $SiO_{2(mono)}$ as the model forced $SiO_{2(mono)}$ concentrations to zero (see for example Fig. 2a and c). In contrast, the supersaturation model was able to capture the equilibrium behavior of the monomeric silica fraction resulting in better mathematical fits for this model. In general, results from the concentration model using the whole data set corroborate the findings by Icopini et al. (2005). Reduced χ^2 values were similar for both the concentration and supersaturation model when fitting the conversion of $SiO_{2(nano)}$ to $SiO_{2(ppt)}$ (k_2) indicating that there is no clear advantage to using either model to fit these data. Problems arose with both models when fitting the $[SiO_{2(ppt)}]$ data at low pH (3–4). The models underestimated the extent of polymerization of monomeric silica in the initial portions of the reaction, leading to artificially high precipitated silica concentrations. This effect is best seen in Fig. 1c, where the concentration model predicts a sharp increase in precipitated silica followed by a sharp decrease and then a gradual increase. However, there is no term in the fitting equations for the consumption of $[SiO_{2(ppt)}]$. This behavior is the direct result of the inability of the concentration model, and to a lesser extent, the supersaturation model, to accurately describe the kinetic behavior of silica under low pH conditions. At higher pH values, where the kinetics of the system are better defined, the models are better able to fit the experimental data (Fig. 2).

4.2. Steady-state behavior

As solubility is a function of particle size, a combination of dissolution-precipitation and polymerization reactions is likely controlling the steady-state silica concentrations as the particles grow in solution (Rimstidt, 1979; Willey, 1980; Crerar et al., 1981). Dissolution of silica from highly-soluble smaller particles can re-precipitate on larger, less soluble particles resulting in an apparent steady-state concentration of monomeric silica in solution. In these experiments, two distinct steady-state concentrations of $SiO_{2(mono)}$ were observed. At higher pH (5–7), monomeric

Table 2
Rate constants for the precipitation of silica (k_2) as predicted by the concentration and supersaturation models

Initial [$SiO_{2(TD)}$] (mmolal)	IS (molal) (±10%)	pH (±0.2)	Concentration model k_2 ($\times 10^{-8}$) (s^{-1}) (±standard error of fit)	Supersaturation model k_2 ($\times 10^{-7}$) (s^{-1}) (±standard error of fit)
20.8	0.01	3	37.0 (20.5)	50.6 (59.3)
		4	349 (121)	167 (71.5)
		5	10,300 (1,820)	1,020 (717)
		6	58,100 (5,560)	5,480 (700)
		7	26.4 (17.4)	146 (11.8)[a]
12.5	0.01	3	4.43 (2.71)	0.509 (0.265)
		4	2.46 (1.20)	4.70 (3.22)
		5	24.4 (11.8)	13.3 (12.6)
		6	115 (32.0)	32.3 (18.5)
		7	1.87 (0.275)	2.53 (0.527)
4.2	0.01	3	195 (378)	13.0 (10.8)
		4	100 (360)	36.4 (30.4)
		5	505 (68.4)	40.5 (6.28)
		6	601 (39.5)	50.4 (3.79)
		7	4,670 (2,880)	6.20 (1,790)
20.8	0.24	3	170 (583)	7,120 (2,430)[a]
		4	110 (37.2)	85.3 (27.9)
		5	640 (43.0)	353 (149)
		6	4,280 (320)	493 (84.1)
		7	19,900 (1,430)	5,530 (986)
12.5	0.24	3	270 (95.6)	43.3 (10.6)
		4	236 (85.9)	20.4 (6.95)
		5	17.7 (31.2)	13.7 (5.25)
		6	1,330 (184)	28.5 (100)
		7	5,140 (288)	1,290 (452)
4.2	0.24	3	528 (691)	605 (198)
		4	1,560 (553)	505 (114)
		5	2,350 (2,510)	35,700 (11,600)
		6	234,000 (109,000)	1,550 (994)
		7	181 (341)	30.4 (20.1)

[a] The kinetics of these data were not well-defined resulting in poor fits. Consequently, these data were not included in the linear regression analyses of the log rate constant vs. pH.

silica concentrations decreased to approximately 2 mmolal, consistent with the predicted equilibrium concentration of amorphous silica at 25 °C (Fig. 2a). At lower pH values (3–4), a steady-state $SiO_{2(mono)}$ concentration of 6 mmolal was often observed (Fig. 1a). When $SiO_{2(mono)}$ concentrations did not reach the amorphous SiO_2 equilibrium concentration (~2.0 mmolal), no significant precipitation occurred. This leads to the inference that a metastable equilibrium is established between the monomeric and nanocolloidal silica fractions under these conditions. This metastable equilibrium concentration is three times higher than the reported equilibrium concentration for bulk amorphous silica in aqueous solutions (Weres et al., 1981; Icehnower and Dove, 2000).

The solubility of amorphous silica in water has been shown to be affected by temperature, particle size, pH, state of internal hydration and the presence of impurities in or absorbed onto the silica particle surface (Iler, 1979). Specifically, for a given type of silica, it has been shown that the solubility increases as the particle size decreases (Alexander, 1957). The Ostwald–Freundlich equation, applied to solubility (also known as the Gibbs–Thompson effect) can be used to relate particle size to solubility as follows:

$$\log_{10}\left[\frac{S_r}{S_i}\right] = 5.7\frac{E}{Td} \tag{11}$$

where S_r is the solubility of a particle of radius r, S_i is the solubility of a particle of infinite radius, E is the interfacial surface energy (ergs cm^{-2}), T is the absolute temperature and d is the particle diameter. Using a value of 80 ergs cm^{-2} for the interfacial surface energy of amorphous silica (Iler, 1973) and 2.0 mmolal for S_i, the diameter of an amorphous silica colloid consistent with the observed 6.0 mmolal equilibrium solubility concentration is found to be ~3 nm. This is in direct agreement with our AFM particle size measurements and strongly suggests that the 6 mmolal concentration represents the equilibrium concentration of amorphous nanocolloidal silica of that particle size.

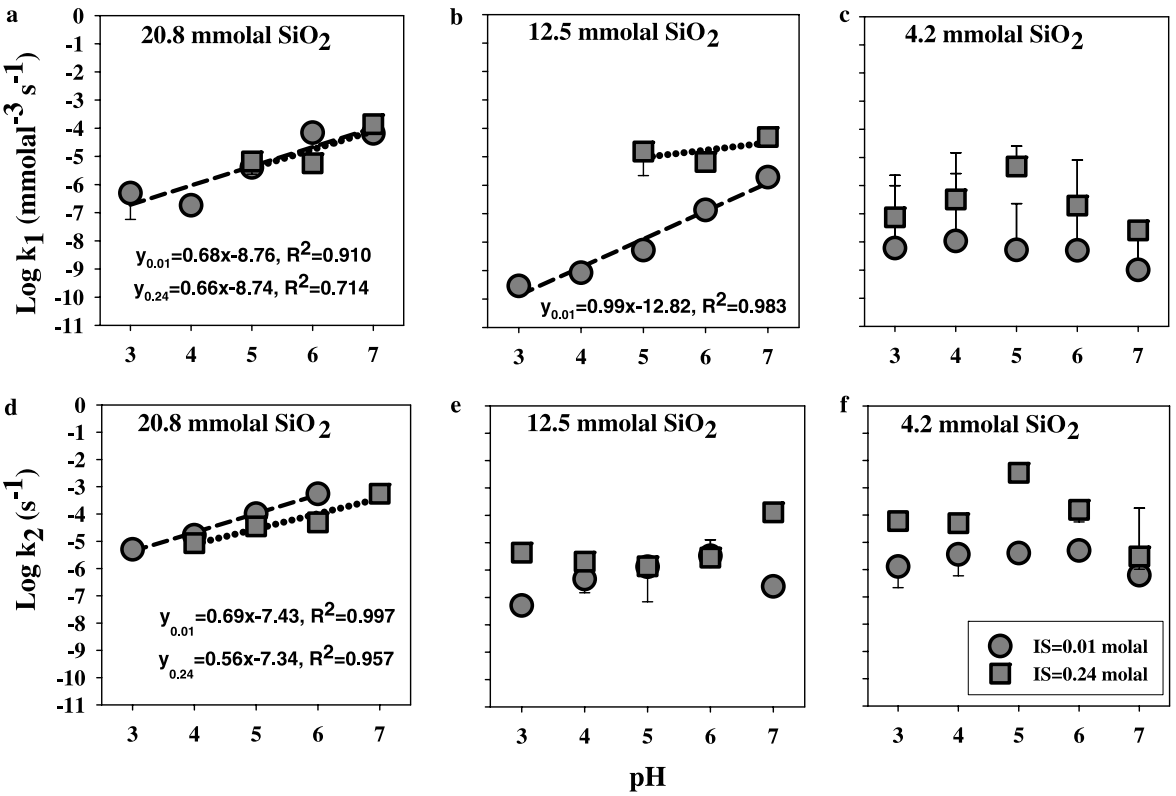

Fig. 5. Log k_1 (top panels) and log k_2 (bottom panels) values determined from the supersaturation model vs. pH for low ionic strength (circles) and high ionic strength (squares) experiments with initial SiO_2 concentrations of (a) 20.8, (b) 12.5 and (c) 4.2 mmolal. Error bars are one standard deviation of the predicted rate constant (when not shown, error bars are on the same scale as the data symbol). Open data symbols represent systems where the kinetics are not sufficiently resolved to predict the reaction rate constants accurately and were not included in the linear fits. Where linear regressions were found to be significant ($p < 0.05$), the equation and correlation coefficient are shown.

4.3. Nanocolloid stability

It is well-known that the stability of silica suspensions contradicts classical DLVO (Deryanin–Landau–Verwey–Overbeek) theory, which predicts that colloidal particles will aggregate quickly when the particles are neutral or weakly charged but will remain in suspension when particles are highly charged (Iler, 1979). In our study, the silica nanocolloids are stable throughout the course of the experiment at low pH where the particles should exhibit little to no surface charge. The k_2 values generally increase with increasing pH and ionic strength with the highest values at high initial SiO_2 concentrations, high ionic strength and near neutral pH (Table 2, Fig. 4d–f and 5d–f). Other studies of silica colloids synthesized under a variety of experimental conditions have also reported increased stability of the silica particles at low pH values where the surface bears little charge (Allen and Matijevic, 1969; Depasse and Watillon, 1970; Higashitani et al., 1991; Kobayashi et al., 2005). Hypothesized reasons for this anomalous behavior include the presence of a repulsive steric force induced by a hairy gel-like surface layer of polysilicic acid chains protruding from the particle surface into solution (Vigil et al., 1994; Zhmud et al., 1998; Adler et al., 2001). The growth of this hairy layer is presumably promoted by aging the particles in water, thereby amplifying the anomalous stability behavior of colloidal silica (Kobayashi et al., 2005).

The presence of counter ions can also affect the reactivity and surface free energy of the nanocolloidal particles formed. This ionic strength effect should decrease as the pH_{pzc} is approached (pH_{pzc} of bulk silica ~2–3). The greatest influence of counter ions in solution was seen at pH 7 in the 20.8 and 12.5 mmolal SiO_2 solutions. Under these conditions, nanocolloidal silica was rapidly and completely converted to precipitated silica. For the same solution conditions but at low IS, the nanocolloidal fraction persisted throughout the course of the experiment and little precipitated silica was formed. However, for many of the conditions studied here, the degree of supersaturation seems to outweigh the effect of ionic strength. For example, at pH 6 and an initial SiO_2 concentration of 12.5 mmolal, the reaction rate constant for the high ionic strength solution is approximately one order of magnitude greater than the rate constant for the low ionic strength solution (Table 2). In contrast, the reaction rate constant for the conversion of $SiO_{2(nano)}$ to $SiO_{2(ppt)}$ in the low IS solution is approximately 500 times greater for an initial SiO_2 concentration of 20.8 mmolal than the corresponding rate constant for the 12.5 mmolal solution. This effect is most pronounced

in the low IS solutions as there is very little difference between the rate constants for the 20.8 and 12.5 mmolal SiO_2 solutions at pH 6 and high IS (Table 2).

AFM images of the stable silica nanocolloids indicate that the primary particles are 3 nm in size (Fig. 3). This is in good agreement with the few previous reports that can be found in the literature (Iler, 1979; Icopini et al., 2005). Using the particle size relationship summarized by Iler (1979), these primary nanocolloids contain ~300 monomeric silica groups. Consistent with our observations, Iler (1979) states that from pH 2 to 7, silica particles will cease to grow after reaching a diameter of 2–3 nm. The larger particles ranging from 30 to 40 nm in diameter present in the AFM image are aggregates of the 3 nm nanocolloids and are not the result of continued growth of the primary particles (Fig. 3). These observations are evidence that aggregation is the primary growth mechanism of silica nanocolloids once the primary particles have been formed.

5. Summary and conclusions

This work provides the first kinetic models for the appearance and evolution of nanocolloidal silica over time under environmentally relevant conditions. Changes in the rate of formation of silica nanocolloids depended on the degree of supersaturation, ionic strength and pH of the experimental solutions while the stability of the nanocolloidal fraction is largely controlled by the pH of the solution. Both the concentration model and the supersaturation model predict similar rate constants for the formation of nanocolloidal and precipitated silica over the range of experimental conditions studied here, although the supersaturation model was able to describe the steady-state behavior of the monomeric fraction resulting in better fits of the monomeric data (k_1). There was no significant improvement in fitting the nanocolloidal data (k_2) with either the concentration or supersaturation model; the reduced χ^2 values were similar for each model.

The presence and behavior of silica nanocolloids has been largely ignored in the geochemical literature. The results from this work indicate that silica nanoparticles can account for a large portion (up to ~65%) of the total silica present in aqueous solutions at low pH (3–4) regardless of ionic strength and also at neutral pH in low ionic strength aqueous systems. Through direct observation and solubility calculations, these nanoparticles appear to be approximately 3 nm in diameter and exhibit a higher equilibrium solubility concentration than the larger, precipitated particles. Over the past few years it has become increasingly recognized that the physical and chemical properties of nanoparticles can be distinctly unique from their bulk phase counterparts due to the increased contribution of surface atoms to the overall composition of these small particles. Little is known about the structure and reactivity of silica nanoparticles and how their properties relate to amorphous silica or quartz mineral phases. The results from this study elucidate the environmental conditions under which the nanocolloidal fraction is important and should be considered when investigating the dissolution and precipitation behavior of silica and silica-based minerals. Further studies aimed at characterizing changes in the particle diameter, structure and reactivity of nanocolloidal silica as they form and grow are needed to more accurately and completely understand their impact on geochemical processes in natural systems.

Acknowledgments

The authors thank three anonymous reviewers whose efforts greatly improved this manuscript. This project was funded by the U.S. Department of Energy (DE-FG07-00ID13954), and The Pennsylvania State University Center for Environmental Kinetics Analysis (NSF EMSI Grant No. CHE-0431382).

Associate editor: William H. Casey

Supplementary data

Supplementary data associated with this article can be found, in the online version, at doi:10.1016/j.gca.2006.10.001.

References

Adler, J.J., Rabinovich, Y.I., Mouldgil, B.M., 2001. Origins of the non-DLVO force between glass surfaces in aqueous solution. *J. Colloid Interface Sci.* **237**, 249–258.

Alexander, G.B., 1954. The polymerization of monosilicic acid. *J. Am. Chem. Soc.* **76**, 2094–2096.

Alexander, G.B., 1957. The effect of particle size on the solubility of amorphous silica in water. *J. Phys. Chem.* **61**, 1563–1564.

Allen, L.H., Matijevic, E., 1969. Stability of colloidal silica: I. effect of simple electrolytes. *J. Colloid Interface Sci.* **31**, 287–296.

Arriagada, F.J., Osseo-Asare, K., 1999. Controlled hydrolysis of tetraethoxysilane in a nonionic water-in-oil microemulsion: a statistical model of silica nucleation. *Colloids Surf. A* **154**, 311–326.

Bogush, G.H., Zukoski IV, C.F., 1991. Uniform silica particle precipitation: an aggregative growth model. *J. Colloid Interface Sci.* **142** (1), 19–34.

Boukari, H., Lin, J.S., Harris, M.T., 1997. Small angle X-ray scattering study of the formation of colloidal silica particles from alkoxides: primary particles or not? *J. Colloid Interface Sci.* **194** (2), 311–318.

Brown Jr., G.E., Henrich, V.E., Casey, W.H., Clark, D.L., Eggleston, C., Felmy, A., Goodman, D.W., Grätzel, M., Maciel, G., McCarthy, M.I., Nealson, K.H., Sverjensky, D.A., Toney, M.F., Zachara, J.M., 1999. Metal oxide surfaces and their interactions with aqueous solutions and microbial organisms. *Chem. Rev.* **99**, 77–174.

Carroll, S., Mroczek, E., Alai, M., Ebert, M., 1998. Amorphous silica precipitation (60 to 120 °C): comparison of laboratory and field rates. *Geochim. Cosmochim. Acta* **62** (8), 1379–1396.

Crerar, D.A., Axtmann, E.V., Axtmann, R.C., 1981. Growth and ripening of silica polymers in aqueous solution. *Geochim. Cosmochim. Acta* **45**, 1259–1266.

Depasse, J., Watillon, A., 1970. The stability of amorphous silica. *J. Colloid Interface Sci.* **33**, 430–438.

Ding, T., Wan, D., Wang, C., Zhang, F., 2004. Silicon isotope compositions of dissolved silicon and suspended matter in the Yangtze River, China. *Geochim. Cosmochim. Acta* **68** (2), 205–216.

Gallup, D.L., 1997. Aluminum silicate scale formation and inhibition: scale characterization and laboratory experiments. *Geothermics* **26** (4), 483–499.

Goto, K., 1956. Effect of pH on polymerization of silicic acid. *J. Phys. Chem.* **60**, 1007–1008.

Gudmundson, S.R., Einarsson, E., 1989. Controlled silica precipitation in geothermal brine at the Reykjanes geo-chemicals plant. *Geothermics* **18** (1/2), 105–112.

Higashitani, K., Kondo, M., Hatade, S., 1991. Effect of particle size on coagulation rate of ultrafine colloidal particles. *J. Colloid Interface Sci.* **142**, 204–213.

Icenhower, J.P., Dove, P.M., 2000. Water behavior at silica surfaces. *Surfactant Sci. Ser.* **90**, 277–295.

Icopini, G.A., Brantley, S.L., Heaney, P.J., 2005. Kinetics of silica oligomerization and nanocolloid formation as a function of pH and ionic strength at 25 °C. *Geochim. Cosmochim. Acta* **69** (2), 293–303.

Iler, R.K., 1973. Colloidal silica. In: Matijevic, E. (Ed.) *Surface and Colloid Science*, vol. 6, pp. 3–100.

Iler, R.K., 1979. *The Chemistry of Silica: Solubility, Polymerization, Colloid and Surface Chemistry, and Biochemistry*. John Wiley & Sons.

Izumi, S., Hara, S., Kumagai, T., Sakai, S., 2005. Molecular dynamics study of homogeneous crystal nucleation in amorphous silicon. *J. Cryst. Growth* **274**, 47–54.

Kobayashi, M., Skarba, M., Gelletto, P., Cakara, D., Borkovec, M., 2005. Effects of heat treatment on the aggregation and charging of Stöber-type silica. *J. Colloid Interface Sci.* **292**, 139–147.

Lee, K., Sathyagal, A.N., McCormick, A.V., 1998. A closer look at an aggregation model of the Stober process. *Colloids Surf. A* **144**, 115–125.

Madras, G., McCoy, B.J., 2005. Nucleation, growth, and coarsening for two- and three-dimensional phase transitions. *J. Cryst. Growth* **279**, 466–476.

Miretzky, P., Conzonno, V., Cirelli, A.F., 2001. Geochemical process controlling silica concentrations in groundwaters of the Salado River drainage basin, Argentina. *J. Geochem. Explor.* **73**, 155–166.

Perry, C.C., Keeling-Tucker, T., 2000. Biosilification: the role of the organic matrix in structure control. *J. Biol. Inorg. Chem.* **5**, 537–550.

Pontoni, D., Narayanan, T., Rennie, A.R., 2002. Time-resolved SAXS study of nucleation and growth of silica colloids. *Langmuir* **18**, 56–59.

Press, W.H., Teukolsky, S.A., Vetterling, W.T., Flannery, B.P., 1992. *Numerical Recipes in C: the Art of Scientific Computing*. Cambridge University Press, Cambridge.

Rajasekaran, R., Rajendiran, K.V., Kumar, R.M., Jayavel, R., Dhanasekaran, D., Ramasamy, P., 2003. Investigation of the nucleation kinetics of zinc thiourea chloride (ZTC) single crystals. *Mat. Chem., Phys.* **82**, 273–280.

Rimstidt, J.D., 1979. *The Kinetics of Silica–Water Reactions*. Ph.D., The Pennsylvania State University.

Rothbaum, H.P., Anderton, B.H., 1975. Removal of silica and arsenic from geothermal discharge waters by precipitation of useful calcium silicates. *Second United Nations Symp. Dev. Use Geother. Resour.*, 1414–1425.

Van Blaaderen, A., Van Geest, J., Vrij, A., 1992. Monodisperse colloidal silica spheres from tetraalkoxysilanes: particle formation and growth mechanism. *J. Colloid Interface Sci.* **154** (2), 481–501.

Vigil, G., Xu, Z., Steinberg, S., Israelachvili, J., 1994. Interactions of silica surfaces. *J. Colloid Interface Sci.* **165**, 367–385.

Vitolo, S., Cialdella, M.L., 1994. Silica separation from reinjection brines at Monte-Amiata geothermal plants, Italy. *Geothermics* **23** (3), 257–266.

Weres, O., Yee, A., Tsao, L., 1981. Kinetics of silica polymerization. *J. Colloid Interface Sci.* **84**, 379–402.

Willey, J.D., 1980. Effects of aging on silica solubility: a laboratory study. *Geochim. Cosmochim. Acta* **44**, 573–578.

Willey, J.D., Spivak, A.J., 1997. Dissolved silica concentrations and reactions in pore waters from continental slope sediments offshore from Cape Hatteras, North Carolina, USA. *Mar. Chem.* **56**, 227–238.

Zhmud, B.V., Meruk, A., Bergstrom, L., 1998. Evaluation of surface ionization parameters from AFM data. *J. Colloid Interface Sci.* **207**, 332–343.